Title:

Boosted coupling of ATP hydrolysis to substrate transport upon cooperative estradiol-17-ß-D-glucuronide binding in a *Drosophila* ABCC transporter

Short title:

Increased coupling by cooperative substrate binding in *Drosophila* ABCC

Authors:

Agnes Karasik[1], Kaitlyn Victoria Ledwitch[2], Tamás Arányi[1], András Váradi[1], Arthur Roberts[2], Flóra Szeri[1#]

[1]Institute of Enzymology, Research Centre for Natural Sciences - Hungarian Academy of Sciences, Budapest, Hungary

[2]Department of Pharmaceutical and Biomedical Sciences, University of Georgia, Athens, USA

[#]Corresponding author, email address: szeri.flora@ttk.mta.hu

Correspondig author:
Flóra Szeri
Active Transport Proteins Research Group
Institute of Enzymology
Research Centre for Natural Sciences
Hungarian Academy of Sciences
Street address: Magyar tudósok körútja 2, H-1117, Budapest, Hungary
Postal address: 1519 Budapest, Pf. 286, Hungary
Phone: +36 306703955
Fax: 3613826700

Current affiliation: Department of Dermatology and Cutaneous Biology,
Sidney Kimmel Medical College, Thomas Jefferson University, Philadelphia,
PA, USA

Funding sources:

This work was supported by the Hungarian Országos Tudományos Kutatási Alapprogramok (OTKA) (Grants 104227 and 114336), Grant VKSz14-1-2015-0155 from theHungarian National Research, Development, and Innovation Office, a grant from the Fulbright Research Scholar by the J. William Fulbright Foreign Scholarship Board, and U.S. National Institutes of Health, National Cancer Institute Grant R01-CA204846-01A1. The authors declare no conflicts of interest.

List of nonstandard abbreviations:

ABC = ATP Binding Cassette

ABCC = ATP-Binding Cassette type-C

ATP = adenosine triphosphate

CDCF = 5-(and-6)-carboxy-2',7'-dichlorofluorescein

COPASI = COmplex PAthway SImulator

DKM = Double KM Mutant

DMRP = Drosophila MRP

DMSO = dimethyl sulfoxide

$E_2$17βD = estradiol-17-ß-D-glucuronide

E2G (in figures) = estradiol-17-ß-D-glucuronide

EGTA = ethylene glycol-bis (2-aminoethylether)-N,N,N′,N′-tetraacetic acid

K_d = dissociation constant

K_M = Michaelis-Menten contstant

MOPS = 3-(N-Morpholino) propanesulfonic acid

MRP = Multidrug Resistance-associated Protein

NBD = nucleotide binding domain

Pi = inorganic phosphate

SDS = sodium dodecyl sulfate

Sf9 = *Spodoptera frugiperda*

T_{max} = maximum transport rate

TMD = transmembrane domain

TRIS = 2-amino-2-(hydroxymethyl)-1,3-propanediol

v_{basal} = basal ATP hydrolysis rate

V_{max} = maximum rate of ATP hydrolysis

Abstract

ABCC (ATP-Binding Cassette type-C) transporters move molecules across cell membranes upon hydrolysis of ATP, however their coupling of ATP hydrolysis to substrate transport remains elusive. Drosophila MRP (DMRP) is the functional ortholog of human long ABCC transporters, with similar substrate and inhibitor specificity but higher activity. Exploiting its high activity, we kinetically dissected the catalytic mechanism of DMRP using estradiol-17-ß-D-glucuronide ($E_2$17βD), the physiological substrate of human ABCCs. We examined DMRP-mediated interdependence of ATP and $E_2$17βD in biochemical assays. We found $E_2$17βD dependent ATPase activity to be biphasic at subsaturating ATP concentrations implying at least two $E_2$17βD binding sites on DMRP. Furthermore, transport measurements indicated strong non-reciprocal cooperativity between ATP and $E_2$17βD. Besides confirming these findings, our kinetic modelling with COmplex PAthway SImulator (COPASI) indicated a ten-fold drop in $E_2$17βD mediated activation of ATP hydrolysis upon saturation of the second $E_2$17βD binding site. Surprisingly, the binding of the second $E_2$17βD allowed substrate transport with constant rate, tightly coupling ATP hydrolysis to transport. In conclusion, we show that the second $E_2$17βD binding, similarly to human ABCC2, allosterically stimulate transport activity of DMRP. Our data suggest that this is achieved by significant increase of coupling of ATP hydrolysis to transport.

Keywords:

Multidrug Resistance-associated Protein (MRP), vanadate-sensitive ATPase activity, E217βD transport, kinetic modelling, COmplex PAthway SImulator (COPASI), allosteric cooperativity

1. Introduction

ABC (ATP Binding Cassette) proteins are present in all kingdoms of life (1). Most eukaryotic ABC proteins are involved in efflux of endo- and xenobiotics across biological membranes utilizing the energy of ATP hydrolysis. The minimal functional unit of ABC transporters is composed of two membrane-spanning transmembrane domains (TMDs) that form binding sites and a translocation pathway for substrates and two cytoplasmic nucleotide binding domains (NBDs) that bind and hydrolyse ATP (2). In the NBDs two molecules of ATP are sandwiched between highly conserved motifs (3), such as Walker A and B of one NBD, and signature motif of the opposing NBD forming two composite catalytic sites in head-to-tail orientation (4-6). NBDs are connected to the TMDs by cytoplasmic loops. It is generally accepted that in the mechanism of ABC transporters ATP binding and hydrolysis is coupled to substrate transport (7). Nucleotide binding and hydrolysis at catalytic centres drive conformational changes of the TMDs resulting in the alternated exposure of the substrate-binding site on each side of the membrane (8) enabling unidirectional solute transport (3, 9). Certain ABC transporters may exhibit uncoupled futile ATP hydrolysis cycles without transport of the substrates or show loose coupling of ATP hydrolysis to solute transport (10-12). The coupling mechanism of ABC transporters is largely unknown.

Members of the C-subfamily of ABC proteins, ABCC transporters, harbour a pair of non-equivalent asymmetric catalytic centres (13-16). The N-terminal catalytic centre is degenerate, in which conserved residues deviate from the generally accepted consensus sequences. The C-terminal catalytic centre agrees with the consensus sequence of ABC transporters. In ABCC transporters there is a unique interdependent asymmetric positive allosteric interaction of the two NBDs, with ATP hydrolysis occurring predominantly at the consensus site, facilitated by ATP binding at the degenerate site (17-20). It has recently been shown that the degenerate site allosterically stabilizes the NBD dimer by preventing its full separation during the transport cycle (20, 21), which is the hallmark of the unique mechanism ABCC transporters (21-26). Despite of the physiological and pathological relevance of ABCC transporters, details of their molecular mechanism remain to be elucidated.

In a subset of ABCC proteins, the so-called long ABCC proteins, in addition to the general core structure of two TMDs and two NBDs, there is an additional trans-membrane domain (TMD_0) N-teminally linked to the core by an intracellular loop (L_0) (24, 27). Long human ABCC transporters (ABCC1, 2, 3, 6 and 10) have key role in the compartmentalization of biologically active endogenous/exogenous compounds, such as inflammatory mediators, hormone derivatives, conjugated bile salts and drug metabolites (28). Furthermore, some are considered to play a role in multidrug resistance in cancer chemotherapy (28, 29). In addition, loss of ABCC2 leads to Dubin-Johnson syndrome characterized by hyperbilirubinemia (30, 31), while mutations of ABCC6 are found in patients with Pseudoxanthoma elasticum (PXE) manifesting soft tissue calcification (32, 33).

Estradiol-17-ß-D-glucuronide ($E_2$17βDG) is a substrate of all but one human long ABCC transporters (ABCC1-3 and 10) (34-38). $E_2$17βDG is the major toxic intermediate of the human estrogene metabolism. Under

physiological conditions it is secreted into the bile mainly *via* ABCC2 (39, 40). In hepatotoxic conditions the level of $E_2$17βDG might be increased, inducing the expression of the sinusoidal ABCC3 (41-43). ABCC3 eliminates toxic compounds, such as $E_2$17βDG, from the hepatocytes into blood thus compensate for the impaired hepatobiliary efflux (44, 45). It has been suggested recently that ABCC2 harbours two $E_2$17βDG binding sites (44, 46). $E_2$17βDG binding to the second allosteric site through positive cooperativity activates the transport of the first bound $E_2$17βDG molecule, or that of another ABCC2 substrate. (44, 46). However, the exact mechanism of this allosteric activation remains to be elucidated.

DMRP is the sole ortholog of long human ABCCs in *Drosophila melanogaster* with high sequence identity and similarity (47-50). DMRP has similar substrate ($E_2$17βDG, leukotriene C_4, 5-(and-6)-Carboxy-2',7'-dichlorofluorescein (CDCF), calcein and fluo3) and inhibitor (probenecid, benzbromarone, indometacin and MK571) specificity to long human ABCC transporters (48). Additionally, reduced expression of endogenous DMRP correlates with decreased secretion of the ABCC1 substrate daunorubicin in Malpighian tubules (51). DMRP in addition plays a role in protection against mercury during fly development (52), which is consistent with inorganic mercury being a substrate of ABCC2 in mice (53). In addition to the shared substrate and inhibitor profile, DMRP exhibits elevated activity in *in vitro* biochemical assays. In the absence of substrates the so called "basal" ATPase activity of human ABCC transporters is low (54) making investigations arduous or impossible. In contrast, DMRP exhibits approximately 15 times higher basal ATPase activity, expressed in the same system (48). DMRP also accomplishes high transport rates. It has one order of magnitude higher activity for $E_2$17βDG, leukotriene C_4 and fluo3 and significantly elevated transport rate for CDCF in comparison to human ABCCs (48, 54). DMRP can be thus considered as a faithful model of human long ABCC transporters, suitable to gain mechanistic insight into processes difficult to study in the human ABCCs.

In the present study we investigated DMRP mediated coupling between ATP hydrolysis and $E_2$17βDG transport. By functional assays and molecular modelling we showed that substrate binding to a second allosteric site highly increases coupling efficiency of these otherwise loosely coupled mechanisms.

2. Materials and methods

2.1. Materials

Restriction endonucleases and T4 ligase were obtained from Thermo Fisher Scientific (Waltham, MA, USA) and New England Biolabs (Ipswich, MA, USA), Pfu polymerase was provided by Strategene (Jolla, CA, USA). Oligonucleotides were ordered from Metabion International AG (Planegg, Germany) and Biological Research Centre of Szeged (Szeged, Hungary). [3H] estradiol-17-ß-D-glucuronide ([3H] E217ßG; 48 Ci/mmol) was purchased from PerkinElmer Life Sciences (Waltham, MA, USA). The anti-DMRP polyclonal antiserum pAB7655, was raised against a synthetic peptide corresponding to amino acids 209-222 of DMRP and was obtained from ZYMED Laboratories Inc. (South San Francisco, CA, USA) as described

previously (47). Secondary HRP-conjugated anti-rabbit antibodies were purchased from Jackson ImmunoResearch (West Grove, PA, USA). Nitrocellulose membrane filters (HWAP00250) were obtained from Millipore (Billerica, MA, United States), and scintillation fluid (Opti-fluor) from PerkinElmer (Waltham, MA, USA). ECL was obtained from Amersham Biosciences (Piscataway, NJ, USA). All other compounds were obtained from Sigma Aldrich (St. Louis, MO, USA). E217βDG was dissolved in DMSO, the final concentration of DMSO in the assay buffer was kept less than 0.1% in transport and less than 1% in ATPase experiments.

2.2. Methods

2.2.1. Generation of constructs

The mutations in the Walker A motifs were generated by Quickchange site-directed mutagenesis. The 8a 4b isoform of *dMRP* cDNA (SD07655) was cloned into pAcUW21L (modified pAcUW vector by Szakács et al.) previously (47). Using this construct, we isolated two DNA fragments containing the sequences of the N- and C- terminal Walker A motifs of *dMRP* by EcoRI-EcoRV and EcoRV and SacI restriction endonucleases. These fragments were cloned into pBluescript KS- vectors, which were used as templates for the PCR mutagenesis reactions. Sequences of the partially overlapping upper and lower primers carrying the mutations of K687M and K1349M were the following:

5’-CGGTTCCGGCATGTCGTCTGTAGTGCAGGCATTCC-3’,

5’-CTACAGACGACATGCCGGAACCGACCGTGCCAACC-3’,

5’-GGTGCCGGCATGTCCAGTCTCACATTGGCCTTGTTCAG-3’,

5’GTGAGACTGGACATGCCGGCACCAGTGCGACCAACAATGC-3’,

respectively. Fragments containing the desired mutations were cloned back into *dMRP* cDNA in pAcUW21L vector with T4 ligase and restriction endonucleases mentioned above, generating double and single Walker A lysine mutant *dMRP* constructs. The presence of the mutation and the fidelity of the sequence of coding region of *dMRP* were confirmed by dideoxy sequencing.

2.2.2. Expression in Sf9 cells, membrane preparation and immunoblotting

Recombinant baculovirus particles containing the dMRP cDNA (SD07655) were prepared as described previously (47). Sf9 cells were cultured and infected with the recombinant baculovirus. After 3-days of virus infection the Sf9 cells were harvested, the membranes were isolated and stored at -70˚C as described previously (55). Total membrane protein concentrations were determined by the modified Lowry method (56). Gel electrophoresis and immunoblotting were performed as described previously (47). Briefly, membrane preparations of Sf9 cells overexpressing wild type or Walker A lysine mutant DMRPs or β-galactosidase (β-gal) containing 5 μg total membrane protein were run on 7.5 % SDS-PAGE gel. Proteins were electro-blotted and

detected by chemo-luminescence using the anti-DMRP polyclonal antiserum pAB7655 (1:500) and HRP conjugated anti-rabbit antibody (1:10000).

2.2.3. Vesicular transport measurements

Vesicular transport measurements with radio-labelled substrates were performed using a rapid filtration method (47). Critical parameters such as incubation time, temperature and the amount of Sf9 vesicles used were determined previously. Parameters that best estimated initial velocities were used in the experiments. Briefly, isolated inside-out Sf9 membrane vesicles containing 100 µg total membrane protein, were incubated at 37 ˚C for 0.5 minutes in the absence or presence of Mg^{2+}ATP of indicated concentration in 150 µl of transport buffer (6 mM $MgCl_2$, 40 mM MOPS-Tris, pH 7.0, 40 mM KCl) at 37°C. Incubation was stopped by the administration of 800 µl of ice-cold washing buffer (40 mM MOPS-TRIS, pH 7.0, 70 mM KCl), after 0.5 min, and samples were instantly filtered through the 0.45 µm pore size nitrocellulose membrane filters (Millipore). Filters were washed twice with 5 ml cold washing buffer and the filter-bound radioactivity was measured in scintillation fluid (Opti-fluor, PerkinElmer) using Wallac 1409 DSA scintillation counter. ATP-dependent transport was calculated by subtracting the values obtained in the absence from those in the presence of ATP.

2.2.4. ATPase activity measurements

The vanadate-sensitive ATPase activity was measured by colorimetric detection of inorganic phosphate liberation as described previously (47, 48, 55). Critical parameters such as incubation time, temperature and the amount of Sf9 vesicles used were determined previously. Conditions that best estimated initial velocities were used in the experiments. In brief, membrane suspensions containing 30 µg (wild type DMRP), 50 µg (K687M) or 100 µg (K1349M, DKM) of total membrane protein were incubated at 37˚C for 5 minutes in 150 µl of a medium containing 40 mM MOPS-Tris, pH 7.0, 0.5 mM EGTA-TRIS, 2 mM dithiothreitol, 50 mM KCl, 5 mM sodium azide, and 1 mM ouabain. The ATPase reaction was started by the addition of Mg^{2+}ATP at indicated concentrations. The reactions were stopped by the addition of 0.1 ml of 5% SDS, and the amounts of inorganic phosphate were determined based on a colorimetric reaction. The optical density was read at 700 nm after 15 min incubation. ATPase activity was calculated as the difference obtained in P_i levels between 0-min reaction (stopped immediately with SDS) and reactions after the indicated incubation periods. Vanadate-sensitive ATPase activities were calculated as the difference between values measured in the presence and in the absence of 1.33 mM vanadate.

2.2.5. Calculation of kinetic parameters of ATPase and vesicular transport measurements

Data were fitted by Michaelis-Menten equation using Igor Pro 6.2 (57-59). Monophasic ATP hydrolysis kinetics was fit to a modified Michaelis Menten Equation (57-59):

$$v = \frac{V_{max}[L]}{K_M + [L]} + v_{basal} \qquad (1)$$

where v is the ATP hydrolysis rate, V_{max} is the maximum ATP hydrolysis rate, v_{basal} is the basal ATP hydrolysis rate, K_M is the Michaelis-Menten contstant and L is the transported substrate. Biphasic ATP hydrolysis kinetics was fit to modified substrate inhibition equation (Equation 2) (57-59):

$$v = \frac{V_{max}}{1 + \frac{K_M}{[L]} + \frac{[L]}{K_i}} + v_{basal} \qquad (2)$$

where K_I is the inhibitory constant. Monophasic transport kinetics was fit another variation of the Michaelis-Menten Equation (57, 58):

$$t = \frac{T_{max}[L]}{K_M + [L]} \qquad (3)$$

where to t is the apparent transport rate and T_{max} is the maximum transport rate.

2.2.6. Kinetic modelling

Transport by ABCC transporters is complex and involves the substrate binding, ATP hydrolysis and transport. Specialized fitting equations can work in some of these complex cases, but often require numerical methods that result in multiple solutions e.g. (60). As a result, a variety of advanced software modelling packages have been developed to fit arbitrary kinetic models including the free Complex Pathway Simulator (COPASI) (61) and the proprietary Berkeley Madonna (University of California, Berkeley, CA). To estimate the discrete microscopic kinetic parameters such as V_{max}s and K_ds the transport and DMRP-mediated ATP hydrolysis in this study were fit to kinetic models using the evolutionary algorithm in the COPASI software as described (59, 61, 62). The software can fit both kinetic and steady state curves with indeterminate number of independent fitting parameters (61).

3. Results

3.1. Catalytic sites of DMRP are functionally non-equivalent.

The conserved Walker A lysine contributes to ATP binding (63) promoting dimerization of the NBDs. Mutation of the N and C-terminal Walker A lysines to methionine alter activity of human ABCC1 differently (13) revealing the functional non-equivalency of the catalytic sites of ABCC proteins. In order to test the functional equality of DMRP we investigated the consequences of single N- or C -terminal or double mutations of the conservative Walker A lysines to methionines, K687M, K1349M and K687M/K1349M referred to as DKM (Double KM Mutant), respectively. The mutant and wild type proteins were overexpressed in *Spodoptera frugiperda* (Sf9) insect cells at comparable levels (Figure 1A) then characterized in functional assays.
The vanadate-sensitive ATPase activities (later referred to as ATPase activity) of K687M, K1349M and DKM proteins were 15%, 3% and 0.8 % of the wild type DMRP, respectively (Figure 1B). In Sf9 membranes

overexpressing the wild type DMRP the vanadate-sensitive ATPase activity was 50% of the total ATPase activity measured in the absence of vanadate. DMRP is known to transport $E_2$17βDG (48). Relative $E_2$17βDG transport rates of the K687M, K1349M and DKM proteins were 48.9%, 13% and 3.7 % of the wild type protein, respectively (Figure 1C). The N-terminal Walker A lysine mutant showed significantly higher activity compared to the C-terminal Walker A mutant while the double Walker A mutant was inactive in functional assays, since $E_2$17βDG uptake in the latter vesicles did not differ significantly from Sf9 vesicles without DMRP expression. These findings support the functional disparity of the two catalytic sites of DMRP and the hypothesis that DMRP shares the same general mechanism of action as its human counterparts (13).

3.2. Non-competitive interaction by E217βDG on ATP hydrolysis depends on substrate saturation of two putative E217βDG binding sites

In order to elucidate kinetic characteristics of the wild type DMRP, we investigated the ATPase cycle of DMRP in the absence and presence of $E_2$17βDG. First, we examined the concentration dependence of ATP and $E_2$17βDG on the DMRP-mediated ATP hydrolysis. Figure 2A shows the hyperbolic ATP hydrolysis rate as a function of ATP concentration. This curve was fit to a modified Michaelis-Menten equation 1. We extracted V_{max} and K_M values from this fitting of 86 +/- 4 nmol Pi/mg membrane protein/min and 0.815 +/- 0.191 mM, respectively. Next, we investigated the effect of ATP on $E_2$17βDG affinity to DMRP (Figure 2B). At saturating 3.33mM ATP concentration, the curve depicting ATPase activity in function of $E_2$17βDG concentration was monophasic, which was in line with our previously published data (48). Fitting the curve to modified Michaelis-Menten equation (Equation 1) gave a K_I (since the ATP hydrolysis is inhibited) and the $V_{max\ basal}$ values of 537+/-336 μM and 67.8+/-2.3 nmol Pi/mg/min, respectively. Interestingly, at subsaturating 0.5 mM ATP concentration, the curve became biphasic, implying binding of at least two molecules of $E_2$17βDG per DMRP monomer. This curve was fit to the substrate inhibition equation (Equation 2). The K_M, V_{max} and the K_I from the fit were 62 +/- 31 μM, 100 +/- 364 nmol Pi/mg/min, and 30.4 +/- 146 μM, respectively. The ATPase activity measured in the presence of the loss of function DKM DMRP was negligible and unaltered by $E_2$17βDG (data not shown).

To get a better handle on $E_2$17βDG and ATP interaction with DMRP, the DMRP-mediated ATP hydrolysis was measured with a range of $E_2$17βDG and in function of ATP concentration (Figure 2C). The apparent DMRP-mediated ATP hydrolysis was monophasic under all conditions, so it was fit to the modified Michaelis-Menten equation (Equation 1). The fitted K_Ms and V_{max}s are shown in Figure 2D on the left and right Y axis for K_M and V_{max}, respectively. The K_M of ATP decreases from 815 +/- 190 μM to 198 +/- 23 μM with increasing concentrations of $E_2$17βDG. This result implies that there is positive cooperativity between $E_2$17βDG and ATP. The V_{max} also decreases from a maximum of 80.79+/-1.25 nmol Pi/mg/min to 25.11+/-0.83 Pi/mg/min.

3.3. Non-reciprocal positive cooperativity of E217βDG toward ATP in the transport cycle of DMRP

ATPase activity in principle is directly linked to transport of substrates in the working mechanism of ABC transporters. Therefore, we investigated whether the putative positive cooperativity detected as an $E_2$17βDG concentration dependent shift of the affinity for ATP found in ATPase activity is characteristic to $E_2$17βDG transport.

First, we determined the $E_2$17βDG transport rate as the function of ATP concentration (Figure 3A) at 10 and 100 μM $E_2$17βDG concentration. We extracted transport kinetic parameters from the monophasic curves fitted to the modified Michaelis-Menten equation (Equation 3). We found that at 100 μM $E_2$17βDG concentration the K_M value for ATP was decreased by a factor of 2.4 relative to the lower $E_2$17βDG concentration (Figure 3B) (697 +/- 93 μM and 293 +/- 38 μM ATP, respectively). This again implied positive cooperativity of $E_2$17βDG towards ATP and reinforced our findings in ATPase activity measurements. Interestingly, though we detected an inhibitory effect of $E_2$17βDG on the rate of ATP hydrolysis, in transport at the higher $E_2$17βDG concentration T_{max} (maximal transport rate) value was increased by a factor of 2.5 relative to the lower $E_2$17βDG concentration (Figure 3B) (470+/-26 to 1198 +/-49 nmol $E_2$17βDG /mg/min for 10 and 100 μM $E_2$17βDG, respectively).

Next, we were interested in the reciprocity of the positive cooperativity of $E_2$17βDG and ATP in transport experiments. Figure 3C shows $E_2$17βDG transport by DMRP in the function of $E_2$17βDG concentration at distinct ATP concentrations. Fitting of the monophasic curves to the modified Michaelis-Menten equation (Equation 3) yielded omissible changes of K_M (48.92+/- 11.7, 46.8 +/- 5.5 and 66.4 +/- 2.5 μM $E_2$17βDG for 0.25, 0.75 and 3.33mM ATP, respectively). Thus, our experiments revealed lack of reciprocity of the positive cooperativity of $E_2$17βDG and ATP in transport measurements. However, increasing concentration of ATP elevated the initial transport rate of $E_2$17βDG with a factor of 3.4 (T_{max} values were 1362+/-112, 3014+/-121 and 4649+/-65 nmol $E_2$17βDG /mg/min for 0.25, 0.75 and 3.33mM ATP, respectively) (Figure 3D).

3.4. Kinetic modelling of the mechanism of DMRP

Our experiments hinted at two potential binding sites for $E_2$17βDG and suggested a unidirectional positive cooperativity for $E_2$17βDG and ATP. The determined global values for the apparent kinetic parameters of ATP hydrolysis and $E_2$17βDG transport did not provide enough detail to resolve the complex catalytic mechanism of DMRP. Therefore, to further dissect the kinetics of DMRP by using the software COPASI we built a kinetic model with two $E_2$17βDG binding sites (Figure 4). Consequent to the two $E_2$17βDG binding sites in our model there are also states for ATP binding in the absence and presence of one or two $E_2$17βDG molecules bound to the transporter. The ATP hydrolysis and transport in the presence of a single and double molecules of $E_2$17βDG are shown on the top of the Figure 4. To obtain the microscopic kinetic parameters such as V_{max}s and K_ds, the

experimentally determined data were fit with COPASI, as described previously (59, 62), using the kinetic model in Figure 4.

3.5. Both E217βDG binding sites are cooperative with ATP binding

Our *in vitro* experiments hinted that there are at least two binding sites for $E_2$17βDG in DMRP. We also found that the apparent K_M of ATP decreased in the presence of $E_2$17βDG implying positive cooperativity with respect to substrate binding (Figure 2D). Since our experiments indicated that there are two molecules of $E_2$17βDG binding to DMRP with putative positive cooperativity, first we fit curves without biasing toward non-cooperative or cooperative models. In case of supposing cooperativity per se we did not know if singly or doubly $E_2$17βDG occupied DMRP is cooperative with ATP. Therefore, we fitted the curves in Figure 2B in Figure 5 to different models for cooperativity. We defined the individual $E_2$17βDG binding sites as "site #1" and "site #2". In Figure 5A, the experimentally determined data points of Figure 2B at 0.5 mM ATP were fit assuming four different models: 1) Both bound $E_2$17βDG molecules are cooperative with bound ATP, 2) $E_2$17βDG bound at "site #1" is cooperative with ATP, 3) $E_2$17βDG bound at "site #2" is cooperative with bound ATP and 4) $E_2$17βDG and ATP are not cooperative. In our calculations, the K_d for ATP was fixed at 815 μM based on the value derived from our *in vitro* experiments (Figure 2A). The values extracted from analysis with COPASI are shown in Table 1. The fits to model #1 and model #2 at subsaturating 0.5 mM ATP concentration gave R-correlation values greater than 0.92, while models #3 and #4 were poor fits. Figure 5B shows the fits of models #1 and #2 to data from Figure 2B at 3.3 mM ATP. Model #1 had an R-correlation of 0.996 and a Chi^2 of 0.31. In contrast, the fit to model #2 had a relatively good R-correlation of 0.971, but the Chi^2 was more than 30-fold higher at 10.35. Therefore, assuming, that the transporter does not switch mechanism upon ATP saturation, model #1, where both $E_2$17βDGs are cooperative, is the most likely interaction of $E_2$17βDG and ATP. Based on best fitting further on we used model #1 for the simulations.

3.6. Saturation of second E217βDG site results in significant drop of ATP hydrolysis rate

We have determined fits by COPASI for DMRP-mediated ATP hydrolysis (Table 2) The K_d of ATP (i.e. K_{d1}) in the absence of $E_2$17βDG was fixed at 815 μM according to our data (Figure 2A). Since we found that both bound $E_2$17βDGs are cooperative with ATP, K_{d2} was made to be equal to K_{d3}, and K_{d4} was made to be equal to K_{d5}. The average R-correlation and Chi^2 values of the fits derived from data referring to ATP hydrolysis were 0.995 and 0.764, respectively, showing that the experimental data correlates well with the model (Table 2). The fitted basal V_{max} (i.e. $V_{max\ basal}$) was 78 +/- 10 nmol/mg/min, which is close to the fit with equation #1 in Figure 2A of 86 +/- 4 nmol/mg/min and is in line with our previous results (48). In the presence of one bound molecule of $E_2$17βDG, the average V_{max} (i.e. V_{max1}) of DMRP-mediated ATP hydrolysis remained constant at 79 +/- 8

nmol/mg/min. With two bound molecules of $E_2$17βDG, the V_{max} (i.e. V_{max2}) declined by almost 90 % to 9 +/- 1 nmol/mg/min.

3.7. Coupling of ATPase to transport is suggested to be highly increased upon saturation of the second E217βDG binding site

ATP hydrolysis kinetics of DMRP was successfully simulated according to model #1. Therefore model #1 was used to obtain transport data in Figures 3A and 3C. The K_d for ATP in the absence of $E_2$17βDG was assumed to be 815 μM. In all cases, the R-correlation was >0.973 and the Chi^2 was less than 0.015 showing good fits. Fits to the normalized transport rates gave V_{max} values of 0.58 and 0.61 nmol $E_2$17βDG/mg membrane protein/min, which reflected relative transport rates with singly and doubly $E_2$17βDG bound DMRP, respectively. Curiously, the transport rates remained constant with $E_2$17βDG, despite of an almost 10-fold decrease in DMRP-mediated ATP hydrolysis. In order to keep the relative transport rate constant under these conditions, there has to be stronger coupling between ATP hydrolysis and $E_2$17βDG, when two molecules of $E_2$17βDG are bound.

3.8. Dissociation constants for the first and second cooperative E217βDG binding sites are similar

The average K_d s (i.e. K_{d2}, $K_{d3\ and}$ K_{d4}, K_{d5}) of $E_2$17βDG cooperatively binding with ATP to site #1 and site #2 determined in ATPase assays were 163 +/-38 μM and 128 +/- 34 μM, respectively (Table 2). The average K_d derived from transport assays in the presence of ATP and a single molecule of $E_2$17βDG (i.e. K_{d2} and K_{d3}) was 141 +/- 19 μM (Table 3). The average K_d value with ATP and two molecules of $E_2$17βDG (K_{d4} and K_{d5}) derived from transport assays was slightly higher at 175 +/- 27 μM (Table 3). K_d values determined from transport experiments correlated well to K_d values derived from ATP hydrolysis experiments. The integrated mean K_d values of ATPase and transport experiments was calculated and depicted in Table 4. The average K_d s of $E_2$17βDG cooperatively binding with ATP to site #1 and site #2 were 155 +/-33 μM and 146 +/- 39 μM, respectively, showing no significant alteration of these dissociation constants.

Experimental data points from Figures 2 and 3 as well as simulated data, obtained with the fitting parameters shown in Table 2 and 3, were plotted in Figure 6 to indicate the quality of simulation.

4. Discussion

In this study, we used the highly active and unique functional orthologue of the long ABCC transporters, DMRP, to shed light on the details of the working mechanism of ABCC proteins. Our analysis revealed the following. The NBDs of DMRP are non-equivalent, resembling those of ABCCs. There are two distinct binding sites for $E_2$17βDG. There is a strong non-reciprocal positive allosteric cooperativity in DMRP with both

$E_2$17βDGs being cooperative towards ATP. DMRP has a highly futile catalytic cycle in terms of $E_2$17βDG transport upon saturation of the first $E_2$17βDG binding site. DMRP exhibits reduced ATP hydrolysis and constant $E_2$17βDG transport rate with tighter coupling of ATPase to $E_2$17βDG transport upon saturation of the second $E_2$17βDG binding site.

In DMRP, similarly to ABCC1, the N-terminal catalytic centre is degenerate, since the Walker B catalytic glutamate is replaced by an aspartate and the corresponding signature motif is also deviated from the consensus LSGGQ to LSVGQ. The C-terminal catalytic centre of DMRP, like that of ABCC1, completely agrees with the consensus sequence of ABC transporters. One of the hallmarks of ABCC transport mechanism is the asymmetric nature of the ATP hydrolysis occurring predominantly at the C-terminal NBD (13, 17). In our experiments lysine to methionine mutation of the C-terminal Walker A almost completely abolished enzyme activity while the analogous mutation of the N-terminal Walker A lysine perturbed ATP hydrolysis and $E_2$17βDG transport at lower extent. The double Walker A mutant DMRP was completely loss of function. Furthermore, we have previously shown that the substrate and inhibitor specificity of DMRP are typical for ABCC (48). This characterisation of DMRP was a prerequisite for its application as a model protein in in-depth analysis of the working mechanism of ABCC transporters.

ABC transporters have an intrinsic ability to hydrolyse ATP even in the absence of their substrates. This intrinsic enzyme activity is often referred to as basal ATPase activity. Basal ATPase activity of the ABC transporters may vary significantly and it is characteristic of the transporter and of the measurement conditions. Transported substrates in principle stimulate the ATPase activity of ABC transporters allowing the coupling of ATP hydrolysis to substrate transport. However, transported substrates have been reported to paradoxically inhibit the ATPase activity of DMRP, a phenomenon that was explained by the existence of a hypothetical endogenous competitive modulator, either a substrate or an allosteric activator, in the Sf9 membranes (48). In line with this, we found that at high ATP saturation the established substrate $E_2$17βDG indeed reduced the ATP hydrolysis rate in a non-competitive manner. However, we found that at partial ATP saturation $E_2$17βDG significantly stimulated the ATPase activity of DMRP, at least in a certain concentration range. These results suggested that $E_2$17βDG and ATP have a complex interaction in the catalytic mechanism of DMRP. In order to elucidate this interaction, we determined ATPase and transport activity as a function of ATP in different $E_2$17βD concentrations. Conversely, we determined ATPase and transport activity as a function of $E_2$17βD in different ATP concentrations (Figure 2 and 3). This novel way to study enzymatic function enabled us to assess the interdependence of the interaction of ATP and $E_2$17βD on the catalytic cycle of DMRP. We found a dynamic concentration-dependent effect of $E_2$17βD on Vmax and K_M for ATP. $E_2$17βD was able to shift the K_M for ATP, however, ATP did not shift the K_M for $E_2$17βD. We consider that our approach used here to characterize allosterically modulated enzyme activity is generally applicable.

Our data obtained with complementary approaches revealed the existence of two cooperative binding sites for $E_2$17βDG with similar dissociation constants. Interestingly, at limiting ATP concentration, the alternative scenario, assuming only the first $E_2$17βDG binding site being cooperative on ATP binding, gave almost as good fit as the best fitting model with two cooperative sites (Figure 5A). This phenomenon suggests that the binding of the first $E_2$17βDG is critical and sufficient for the cooperativity at low ATP saturation. At this ATP concentration, based on analogy to human ABCC transporters, only the non-canonical degenerate NBD is supposed to be saturated with ATP (17-19, 64). Therefore, it is plausible that the first $E_2$17βDG binding site is cooperative with the N-terminal NBD. In contrast, at excess ATP concentration the alternative model, with the first $E_2$17βDG binding being cooperative only, failed to give a good fit of the experimental data (Figure 5B). This implies that the saturation of the second $E_2$17βDG binding site is indispensable for cooperativity at high ATP saturation. Presumably, the second $E_2$17βDG binding site cooperates with the C-terminal canonical NBD, which is saturated only at excess ATP concentrations. Interestingly, saturation of the second $E_2$17βDG binding site, on a non-competitive manner, reduced rate constant for ATP hydrolysis by 90 percent, suggesting allostery-driven inhibition of ATP hydrolysis.

Consequent to the two substrate binding sites, two distinct transport rates were distinguishable in our kinetic model. Surprisingly, in contrast to the one order of magnitude difference in the rate constants for ATP hydrolysis, the transport rate was not altered upon saturation of the second $E_2$17βDG binding site. At saturation of solely the first $E_2$17βDG binding site, DMRP exhibited almost entirely futile ATPase cycles, with approximately 180 ATP hydrolysed upon transport of a single $E_2$17βDG, supposing one molecule of ATP hydrolysed per cycle. In contrast, at excess $E_2$17βDG saturation, as the rate constant for ATP hydrolysis dropped one order of magnitude while $E_2$17βDG transport rate remained constant, coupling of ATP hydrolysis to transport was elevated by an order of magnitude. This gave a ratio of approximately 18 ATP hydrolysed per each $E_2$17βDG transported, supposing a single ATP is hydrolysed per catalytic cycle and one $E_2$17βDG molecule is transported per transport cycle. The allosterically driven boost of efficiency of $E_2$17βDG transport is achieved by hydrolysing less ATP with a maintained transport rate instead of transporting more substrate upon maintained level of ATP hydrolysis.

The close homologue of DMRP, human ABCC2, also harbours two binding sites for $E_2$17βDG (44, 46). Transport of the first $E_2$17βDG molecule bound to the transport site is allosterically stimulated by binding of the second $E_2$17βDG to the allosteric site (46). However, for ABCC2 the mechanism of allosteric stimulation is not yet known. The phenomenon, that DMRP changes its coupling ratio at high extent depending on the saturation of an allosteric substrate binding site, is a remarkable finding. Taking the high level of sequential and functional homology of DMRP to human ABCC2 into account, our results raise the possibility that the reported allosteric stimulation of $E_2$17βDG transport in ABCC2 might be achieved by allostery-driven tighter coupling of ATP hydrolysis to transport.

The asymmetry in the effect of substrate binding to its distinct binding sites might be a characteristic feature of ABCC proteins. This could lead to an intimately orchestrated collaboration of substrates and non-equal catalytic centres and might also be relevant to co-transport of molecules, a phenomenon often found in the physiology of ABCCs. In conclusion, our work proposes allostery-driven boosting of coupling of ATP hydrolysis to transport as a relevant mechanism for ABCC transporters.

5. Author Contributions

F. Szeri designed research; A. Karasik and F. Szeri performed research; F Szeri, A. Roberts, A. Karasik and K. Ledwitch analysed data; F. Szeri, A. Roberts, T. Aranyi, A. Karasik and A. Varadi, and wrote the paper.

6. Acknowledgements:

This work was funded and supported by the Hungarian OTKA grants 104227 and 114336, the Hungarian VKSz14-1-2015-0155 grant and the R01CA204846-01A1 grant of the National Cancer Institute of USA. We would like to thank to Steven Robinow for sharing the plasmid with the wild type DMRP sequence and for the primary antibody against DMRP. We also would like to thank Károly Liliom and Gergely Szakács for their insightful comments.

The assistance of Györgyi Demeter is also greatly acknowledged.

7. References

1. Higgins, C. F. (1992) ABC transporters: from microorganisms to man. *Annu Rev Cell Biol* **8**, 67-113
2. Hyde, S. C., Emsley, P., Hartshorn, M. J., Mimmack, M. M., Gileadi, U., Pearce, S. R., Gallagher, M. P., Gill, D. R., Hubbard, R. E., and Higgins, C. F. (1990) Structural model of ATP-binding proteins associated with cystic fibrosis, multidrug resistance and bacterial transport. *Nature* **346**, 362-365
3. Smith, P. C., Karpowich, N., Millen, L., Moody, J. E., Rosen, J., Thomas, P. J., and Hunt, J. F. (2002) ATP Binding to the Motor Domain from an ABC Transporter Drives Formation of a Nucleotide Sandwich Dimer. *Mol Cell* **10**, 139-149
4. Hung, L. W., Wang, I. X., Nikaido, K., Liu, P. Q., Ames, G. F., and Kim, S. H. (1998) Crystal structure of the ATP-binding subunit of an ABC transporter. *Nature* **396**, 703-707
5. Jones, P. M., and George, A. M. (1999) Subunit interactions in ABC transporters: towards a functional architecture. *FEMS Microbiol Lett* **179**, 187-202
6. Locher, K. P., Lee, A. T., and Rees, D. C. (2002) The E. coli BtuCD structure: a framework for ABC transporter architecture and mechanism. *Science* **296**, 1091-1098
7. Shapiro, A. B., and Ling, V. (1998) The mechanism of ATP-dependent multidrug transport by P-glycoprotein. *Acta Physiol Scand Suppl* **643**, 227-234
8. Jones, P. M., O'Mara, M. L., and George, A. M. (2009) ABC transporters: a riddle wrapped in a mystery inside an enigma. *Trends Biochem Sci* **34**, 520-531
9. Dawson, R. J., and Locher, K. P. (2006) Structure of a bacterial multidrug ABC transporter. *Nature* **443**, 180-185
10. Al-Shawi, M. K., Polar, M. K., Omote, H., and Figler, R. A. (2003) Transition State Analysis of the Coupling of Drug Transport to ATP Hydrolysis by P-glycoprotein.

11. Ernst, R., Kueppers, P., Klein, C. M., Schwarzmueller, T., Kuchler, K., and Schmitt, L. (2008) A mutation of the H-loop selectively affects rhodamine transport by the yeast multidrug ABC transporter Pdr5. *Proc Natl Acad Sci U S A* **105**, 5069-5074
12. Perez, C., Kohler, M., Janser, D., Pardon, E., Steyaert, J., Zenobi, R., and Locher, K. P. (2017) Structural basis of inhibition of lipid-linked oligosaccharide flippase PglK by a conformational nanobody. *Sci Rep* **7**, 46641
13. Gao, M., Cui, H. R., Loe, D. W., Grant, C. E., Almquist, K. C., Cole, S. P., and Deeley, R. G. (2000) Comparison of the functional characteristics of the nucleotide binding domains of multidrug resistance protein 1. *J Biol Chem* **275**, 13098-13108
14. Nagata, K., Nishitani, M., Matsuo, M., Kioka, N., Amachi, T., and Ueda, K. (2000) Nonequivalent nucleotide trapping in the two nucleotide binding folds of the human multidrug resistance protein MRP1. *J Biol Chem* **275**, 17626-17630
15. Matsuo, M., Kioka, N., Amachi, T., and Ueda, K. (1999) ATP binding properties of the nucleotide-binding folds of SUR1. *J Biol Chem* **274**, 37479-37482
16. Cole, S., Bhardwaj, G., Gerlach, J., Mackie, J., Grant, C., Almquist, K., Stewart, A., Kurz, E., Duncan, A., and Deeley, R. (1992) Overexpression of a transporter gene in a multidrug-resistant human lung cancer cell line.
17. Hou, Y. X., Cui, L., Riordan, J. R., and Chang, X. B. (2002) ATP binding to the first nucleotide-binding domain of multidrug resistance protein MRP1 increases binding and hydrolysis of ATP and trapping of ADP at the second domain. *J Biol Chem* **277**, 5110-5119
18. Hou, Y. X., Riordan, J. R., and Chang, X. B. (2003) ATP binding, not hydrolysis, at the first nucleotide-binding domain of multidrug resistance-associated protein MRP1 enhances ADP.Vi trapping at the second domain. *J Biol Chem* **278**, 3599-3605
19. Hou, Y.-x., Cui, L., Riordan, J. R., and Chang, X.-b. (2000) Allosteric Interactions between the Two Non-equivalent Nucleotide Binding Domains of Multidrug Resistance Protein MRP1.
20. Hohl, M., Hurlimann, L. M., Bohm, S., Schoppe, J., Grutter, M. G., Bordignon, E., and Seeger, M. A. (2014) Structural basis for allosteric cross-talk between the asymmetric nucleotide binding sites of a heterodimeric ABC exporter. *Proc Natl Acad Sci U S A* **111**, 11025-11030
21. Timachi, M. H., Hutter, C. A., Hohl, M., Assafa, T., Bohm, S., Mittal, A., Seeger, M. A., and Bordignon, E. (2017) Exploring conformational equilibria of a heterodimeric ABC transporter. *Elife* **6**
22. Bakos, E., and Homolya, L. (2007) Portrait of multifaceted transporter, the multidrug resistance-associated protein 1 (MRP1/ABCC1). *Pflugers Arch* **453**, 621-641
23. Procko, E., Ferrin-O'Connell, I., Ng, S. L., and Gaudet, R. (2006) Distinct structural and functional properties of the ATPase sites in an asymmetric ABC transporter. *Mol Cell* **24**, 51-62
24. Deeley, R. G., Westlake, C., and Cole, S. P. (2006) Transmembrane transport of endo- and xenobiotics by mammalian ATP-binding cassette multidrug resistance proteins. *Physiol Rev* **86**, 849-899
25. Payen, L. F., Gao, M., Westlake, C. J., Cole, S. P. C., and Deeley, R. G. (2003) Role of Carboxylate Residues Adjacent to the Conserved Core Walker B Motifs in the Catalytic Cycle of Multidrug Resistance Protein 1 (ABCC1).
26. Zhang, X. C., Han, L., and Zhao, Y. (2016) Thermodynamics of ABC transporters. In *Protein Cell* Vol. 7 pp. 17-27
27. Tusnady, G. E., Bakos, E., Varadi, A., and Sarkadi, B. (1997) Membrane topology distinguishes a subfamily of the ATP-binding cassette (ABC) transporters. *FEBS Lett* **402**, 1-3
28. Slot, A. J., Molinski, S. V., and Cole, S. P. (2011) Mammalian multidrug-resistance proteins (MRPs). *Essays Biochem* **50**, 179-207
29. Hopper-Borge, E. A., Churchill, T., Paulose, C., Nicolas, E., Jacobs, J. D., Ngo, O., Kuang, Y., Grinberg, A., Westphal, H., Chen, Z. S., Klein-Szanto, A. J., Belinsky, M. G., and Kruh, G. D. (2011) Contribution of Abcc10 (Mrp7) to in vivo paclitaxel resistance as assessed in Abcc10(-/-) mice. *Cancer Res* **71**, 3649-3657

30. Paulusma, C. C., Bosma, P. J., Zaman, G. J. R., Bakker, C. T. M., Otter, M., Scheffer, G. L., Scheper, R. J., Borst, P., and Elferink, R. P. J. O. (1996) Congenital Jaundice in Rats with a Mutation in a Multidrug Resistance-Associated Protein Gene.
31. Mayer, R., Kartenbeck, J., Buchler, M., Jedlitschky, G., Leier, I., and Keppler, D. (1995) Expression of the MRP gene-encoded conjugate export pump in liver and its selective absence from the canalicular membrane in transport-deficient mutant hepatocytes. *J Cell Biol* **131**, 137-150
32. Li, Q., Aranyi, T., Varadi, A., Terry, S. F., and Uitto, J. (2016) Research Progress in Pseudoxanthoma Elasticum and Related Ectopic Mineralization Disorders. *J Invest Dermatol* **136**, 550-556
33. Jansen, R. S., Duijst, S., Mahakena, S., Sommer, D., Szeri, F., Varadi, A., Plomp, A., Bergen, A. A., Oude Elferink, R. P., Borst, P., and van de Wetering, K. (2014) ABCC6-mediated ATP secretion by the liver is the main source of the mineralization inhibitor inorganic pyrophosphate in the systemic circulation-brief report. *Arterioscler Thromb Vasc Biol* **34**, 1985-1989
34. Loe, D. W., Almquist, K. C., Cole, S. P., and Deeley, R. G. (1996) ATP-dependent 17 beta-estradiol 17-(beta-D-glucuronide) transport by multidrug resistance protein (MRP). Inhibition by cholestatic steroids. *J Biol Chem* **271**, 9683-9689
35. Zeng, H., Liu, G., Rea, P. A., and Kruh, G. D. (2000) Transport of amphipathic anions by human multidrug resistance protein 3. *Cancer Res* **60**, 4779-4784
36. Cui, Y., Konig, J., Buchholz, J. K., Spring, H., Leier, I., and Keppler, D. (1999) Drug resistance and ATP-dependent conjugate transport mediated by the apical multidrug resistance protein, MRP2, permanently expressed in human and canine cells. *Mol Pharmacol* **55**, 929-937
37. Chen, Z. S., Hopper-Borge, E., Belinsky, M. G., Shchaveleva, I., Kotova, E., and Kruh, G. D. (2003) Characterization of the transport properties of human multidrug resistance protein 7 (MRP7, ABCC10). *Mol Pharmacol* **63**, 351-358
38. Keppler, D., Leier, I., and Jedlitschky, G. (1997) Transport of glutathione conjugates and glucuronides by the multidrug resistance proteins MRP1 and MRP2. *Biol Chem* **378**, 787-791
39. Vore, M., Liu, Y., and Huang, L. (1997) Cholestatic properties and hepatic transport of steroid glucuronides. *Drug Metab Rev* **29**, 183-203
40. Takikawa, H., Yamazaki, R., Sano, N., and Yamanaka, M. (1996) Biliary excretion of estradiol-17 beta-glucuronide in the rat. *Hepatology* **23**, 607-613
41. Donner, M. G., and Keppler, D. (2001) Up-regulation of basolateral multidrug resistance protein 3 (Mrp3) in cholestatic rat liver. *Hepatology* **34**, 351-359
42. Hitzl, M., Klein, K., Zanger, U. M., Fritz, P., Nüssler, A. K., Neuhaus, P., and Fromm, M. F. (2003) Influence of Omeprazole on Multidrug Resistance Protein 3 Expression in Human Liver.
43. Scheffer, G. L., Kool, M., de Haas, M., de Vree, J. M., Pijnenborg, A. C., Bosman, D. K., Elferink, R. P., van der Valk, P., Borst, P., and Scheper, R. J. (2002) Tissue distribution and induction of human multidrug resistant protein 3. *Lab Invest* **82**, 193-201
44. Bodo, A., Bakos, E., Szeri, F., Varadi, A., and Sarkadi, B. (2003) Differential modulation of the human liver conjugate transporters MRP2 and MRP3 by bile acids and organic anions. *J Biol Chem* **278**, 23529-23537
45. Bodo, A., Bakos, E., Szeri, F., Varadi, A., and Sarkadi, B. (2003) The role of multidrug transporters in drug availability, metabolism and toxicity. *Toxicol Lett* **140-141**, 133-143
46. Gerk, P. M., Li, W., and Vore, M. (2004) ESTRADIOL 3-GLUCURONIDE IS TRANSPORTED BY THE MULTIDRUG RESISTANCE-ASSOCIATED PROTEIN 2 BUT DOES NOT ACTIVATE THE ALLOSTERIC SITE BOUND BY ESTRADIOL 17-GLUCURONIDE.
47. Tarnay, J. N., Szeri, F., Ilias, A., Annilo, T., Sung, C., Le Saux, O., Varadi, A., Dean, M., Boyd, C. D., and Robinow, S. (2004) The dMRP/CG6214 gene of Drosophila is evolutionarily and functionally related to the human multidrug resistance-associated protein family. *Insect Mol Biol* **13**, 539-548
48. Szeri, F., Ilias, A., Pomozi, V., Robinow, S., Bakos, E., and Varadi, A. (2009) The high turnover Drosophila multidrug resistance-associated protein shares the biochemical features of its human orthologues. *Biochim Biophys Acta* **1788**, 402-409

49. Grailles, M., Brey, P. T., and Roth, C. W. (2003) The Drosophila melanogaster multidrug-resistance protein 1 (MRP1) homolog has a novel gene structure containing two variable internal exons. *Gene* **307**, 41-50
50. Dermauw, W., and Van Leeuwen, T. (2014) The ABC gene family in arthropods: comparative genomics and role in insecticide transport and resistance. *Insect Biochem Mol Biol* **45**, 89-110
51. Chahine, S., Seabrooke, S., and O'Donnell, M. J. (2012) Effects of genetic knock-down of organic anion transporter genes on secretion of fluorescent organic ions by Malpighian tubules of Drosophila melanogaster. *Arch Insect Biochem Physiol* **81**, 228-240
52. Prince, L., Korbas, M., Davidson, P., Broberg, K., and Rand, M. D. (2014) Target Organ Specific Activity of Drosophila MRP (ABCC1) Moderates Developmental Toxicity of Methylmercury. *Toxicol Sci* **140**, 425-435
53. Bridges, C. C., Joshee, L., van den Heuvel, J. J., Russel, F. G., and Zalups, R. K. (2013) Glutathione status and the renal elimination of inorganic mercury in the Mrp2(-/-) mouse. *PLoS One* **8**, e73559
54. Bakos, E., Evers, R., Sinko, E., Varadi, A., Borst, P., and Sarkadi, B. (2000) Interactions of the human multidrug resistance proteins MRP1 and MRP2 with organic anions. *Mol Pharmacol* **57**, 760-768
55. Sarkadi, B., Price, E. M., Boucher, R. C., Germann, U. A., and Scarborough, G. A. (1992) Expression of the human multidrug resistance cDNA in insect cells generates a high activity drug-stimulated membrane ATPase. *J Biol Chem* **267**, 4854-4858
56. Bensadoun, A., and Weinstein, D. (1976) Assay of proteins in the presence of interfering materials. *Anal Biochem* **70**, 241-250
57. Segel, I. H. (1993) *Enzyme Kinetics: Behavior and Analysis of Rapid Equilibrium and Steady-State Enzyme Systems*
58. Roberts, A. G., Yang, J., Halpert, J. R., Nelson, S. D., Thummel, K. T., and Atkins, W. M. (2011) The structural basis for homotropic and heterotropic cooperativity of midazolam metabolism by human cytochrome P450 3A4. *Biochemistry* **50**, 10804-10818
59. Ledwitch, K. V., Gibbs, M. E., Barnes, R. W., and Roberts, A. G. (2016) Cooperativity between verapamil and ATP bound to the efflux transporter P-glycoprotein. *Biochem Pharmacol* **118**, 96-108
60. Davydov, D. R., Botchkareva, A. E., Davydova, N. E., and Halpert, J. R. (2005) Resolution of two substrate-binding sites in an engineered cytochrome P450eryF bearing a fluorescent probe. *Biophys J* **89**, 418-432
61. Hoops, S., Sahle, S., Gauges, R., Lee, C., Pahle, J., Simus, N., Singhal, M., Xu, L., Mendes, P., and Kummer, U. (2006) COPASI--a COmplex PAthway SImulator. *Bioinformatics* **22**, 3067-3074
62. Ledwitch, K. V., Barnes, R. W., and Roberts, A. G. (2016) Unravelling the complex drug-drug interactions of the cardiovascular drugs, verapamil and digoxin, with P-glycoprotein. *Biosci Rep* **36**
63. Walker, J. E., Saraste, M., Runswick, M. J., and Gay, N. J. (1982) Distantly related sequences in the alpha- and beta-subunits of ATP synthase, myosin, kinases and other ATP-requiring enzymes and a common nucleotide binding fold. *Embo j* **1**, 945-951
64. Yang, R., Cui, L., Hou, Y. X., Riordan, J. R., and Chang, X. B. (2003) ATP binding to the first nucleotide binding domain of multidrug resistance-associated protein plays a regulatory role at low nucleotide concentration, whereas ATP hydrolysis at the second plays a dominant role in ATP-dependent leukotriene C4 transport. *J Biol Chem* **278**, 30764-30771

8. Figure and Table legends

Figure 1. Catalytic sites of DMRP are functionally non-equivalent

A: Expression of wild-type and mutant DMRPs in insect cells. Immunoblot of membrane preparations of Sf9 cells overexpressing wild type or N- or C-terminal single- or double- Walker A lysine mutant DMRPs or β-galactosidase (β-gal). **B: Vanadate-sensitive basal ATPase activity of wild type and Walker A lysine**

mutant DMRPs in Sf9 inside-out vesicles. Activities were measured in the presence of 3.33 mM Mg^{2+}ATP using 30, 50, and 100-100 μg total membrane protein containing Sf9 membrane preparations overexpressing wild-type, K687M, K1349M and DKM DMRP, respectively. **C: ATP-dependent $E_2$17βDG transport of wild type and Walker A lysine mutant DMRPs** measured in the presence or absence of 4 mM Mg^{2+}ATP at 100 μM $E_2$17βDG concentration.

Panels B and C depict the mean values of at least three independent experiments done in at least duplicates and error bars show the standard error of the estimate of mean value (S.E.M.). Activities were normalized to that of the wild type protein.

Figure 2. Complex interaction of $E_2$17βDG and ATP in ATPase activity of wild type DMRP

A: Basal ATPase activity as the function of Mg^{2+}ATP; **B: ATPase activity as a function of $E_2$17βDG concentration** in the presence of **3.33 mM Mg^{2+}ATP** (closed diamonds, solid line) and in the presence of **0.5mM Mg^{2+}ATP** (open diamonds, dashed line). **C: ATPase activity** in the absence or presence of various concentrations of **$E_2$17βDG** plotted **as a function of Mg^{2+}ATP** concentration. Panels A, B and C depict mean values of at least three independent experiments done in at least duplicates. Error bars show the standard error of the estimate of mean value (S.E.M.). **D: K_M** (open squares and dashed line, left Y axis) **and V_{max}** (closed squares and solid line, right Y axis) **for ATP** in ATPase activity extracted from fits of panel C. Error bars show the standard deviation of mean value (S.D).

Figure 3. Non-reciprocal cooperativity of $E_2$17βDG and ATP indicated in transport activity

A: $E_2$17βDG transport as the **function of Mg^{2+}ATP** concentration in the presence of **100 μM** (closed diamonds, solid line) and **10μM** (open diamonds, dashed line) **$E_2$17βDG**; **B: K_M** (open squares and dashed line, left Y axis) **and *Tmax*** (closed squares and solid line, right Y axis) **for ATP** in transport activity as the **function of $E_2$17βDG** concentration extracted from fits of panel A.; **C: $E_2$17βDG transport as the function of $E_2$17βDG** concentration measured in the presence of **0.25, 0.75 and 3.33mM Mg^{2+}ATP**. **D: K_M** (open squares and dashed line, left Y axis) **and *Tmax*** (closed squares and solid line, right Y axis) **for $E_2$17βDG** in transport activity **as a function of Mg^{2+}ATP** concentration extracted from fits of panel C; Panels A and C depict mean values of at least three independent experiments done in at least duplicates. Error bars show the standard error of the estimate of mean value (S.E.M.).; Panels B and D depict extracted mean values, error bars show the standard deviation of mean value (S.D.).

Figure 4. Kinetic model of wild type DMRP

E refers to DMRP, S_i to transported substrate ($E_2$17βDG) at the inward facing binding site, S_o to transported substrate at the outward facing binding site. When location of substrate is indispensable it is indicated by $S_?$. Binding of $E_2$17βDG is indicated with dotted arrow, binding of ATP is indicated with solid arrow, ATP

hydrolysis is indicated with dashed arrow and transport of $E_2$17βDG is indicated with double arrow. Kinetic parameters are depicted in italics and refer to dissociation constants for ATP (K_{d1}, K_{d3}, K_{d5}), $E_2$17βDG (K_{d2}, K_{d4}), initial rate of ATP hydrolysis in the absence of $E_2$17βDG ($V_{max\ basal}$) or in the presence of one or two molecules of $E_2$17βDG (V_{max1}, V_{max2}), respectively as well as initial rate of $E_2$17βDG transport in the presence of one or two molecules of $E_2$17βDG (T_1, T_2), respectively.

Figure 5. Fit of experimental values and modelled scenarios for cooperativity

A: Fit of the simulated ATPase activity of the 4 different scenarios (model#1-4, solid, dashed, dotted and dashed/dotted lines, respectively) (see Table 1) to the experimental values (open squares) from Figure 2B at limiting (0.5mM) ATP concentration.

B: Fit of the simulated ATPase activity of model#1 and 2 (solid line and dashed line), respectively (see Table 1) to the experimental values (closed squares) from Figure 2B at excess (3.33mM) ATP concentration.

Figure 6. Fit of the normalised experimental values and the corresponding simulated values derived from modelling in COPASI

Symbols indicate experimental values while simulated data from Table 2 and 3 are depicted as lines. **A: ATPase activity as a function of $E_2$17βDG concentration** at limiting and excess ATP concentrations normalised to $V_{max\ basal}$ determined at excess ATP. **B: ATPase activity as a function of ATP concentration** with various $E_2$17βDG concentrations normalised to $V_{max\ basal}$ determined at excess ATP. **C: $E_2$17βDG transport activity as a function of $E_2$17βDG concentration** at different ATP concentrations normalised to *Tmax* of $E_2$17βDG transport determined at excess ATP concentration. **D: $E_2$17βDG transport activity as a function of ATP concentration** at different $E_2$17βDG concentrations normalised to *Tmax* of $E_2$17βDG transport determined at excess ATP concentration.

Table 1. Cooperativity of $E_2$17βDG and ATP at limiting and excess ATP concentrations modelled in COPASI

Kinetic parameters referring to ATPase activity were modelled using 4 different scenarios for limiting ATP concentration (0.5mM ATP): model#1: both ATP binding are cooperative ($K_{d2}=K_{d3}$; $K_{d4}=K_{d5}$); model#2: first ATP binding is cooperative ($K_{d2}=K_{d3}$); model#3: second ATP binding is cooperative ($K_{d4}=K_{d5}$); model#4: none of the ATP bindings are cooperative. Kinetic parameters referring to ATPase activity were modelled using 2 different scenarios for excess ATP concentration (3.3mM ATP): model#1: both ATP binding are cooperative ($K_{d2}=K_{d3}$; $K_{d4}=K_{d5}$); model#2: first ATP binding is cooperative ($K_{d2}=K_{d3}$); To show quality of the fits the R and Chi^2 values are also provided.

Table 2. Kinetic parameters of ATP hydrolysis determined by modelling in COPASI

Kinetic parameters for ATP hydrolysis of wild type DMRP were calculated using COPASI software, based on the kinetic model#1 represented in Figure 4. The R and Chi^2 values of the fits are also provided.

Table 3. Kinetic parameters of $E_2$17βDG transport determined by modelling in COPASI

Kinetic parameters for $E_2$17βDG transport of wild type DMRP were calculated using COPASI software, based on the kinetic model#1 represented in Figure 4. The R and Chi^2 values of the fits are also provided.

Table 4. Integrated kinetic parameters of ATPase activity and $E_2$17βDG transport

The mean values of the kinetic parameters of Table 2 and 3 were calculated and presented as integrated activity. R and Chi^2 values of the fits are also provided.

Figure 1.

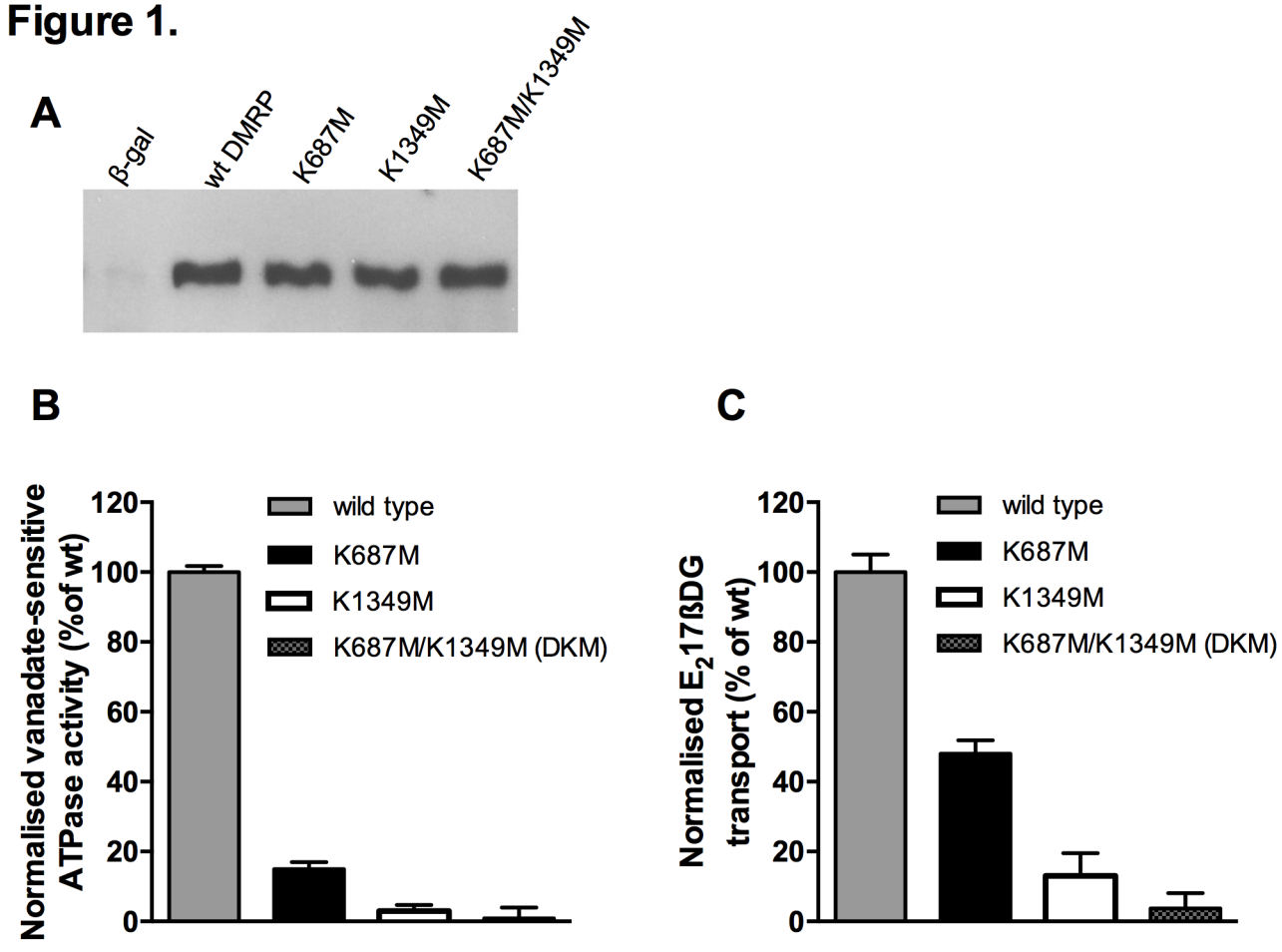
A
β-gal
wt DMRP
K687M
K1349M
K687M/K1349M
B
Normalised vanadate-sensitive ATPase activity (%of wt)
120
100
80
60
40
20
0
wild type
K687M
K1349M
K687M/K1349M (DKM)
C
Normalised E2 17ßDG transport (% of wt)
120
100
80
60
40
20
0
wild type
K687M
K1349M
K687M/K1349M (DKM)

Figure 2.

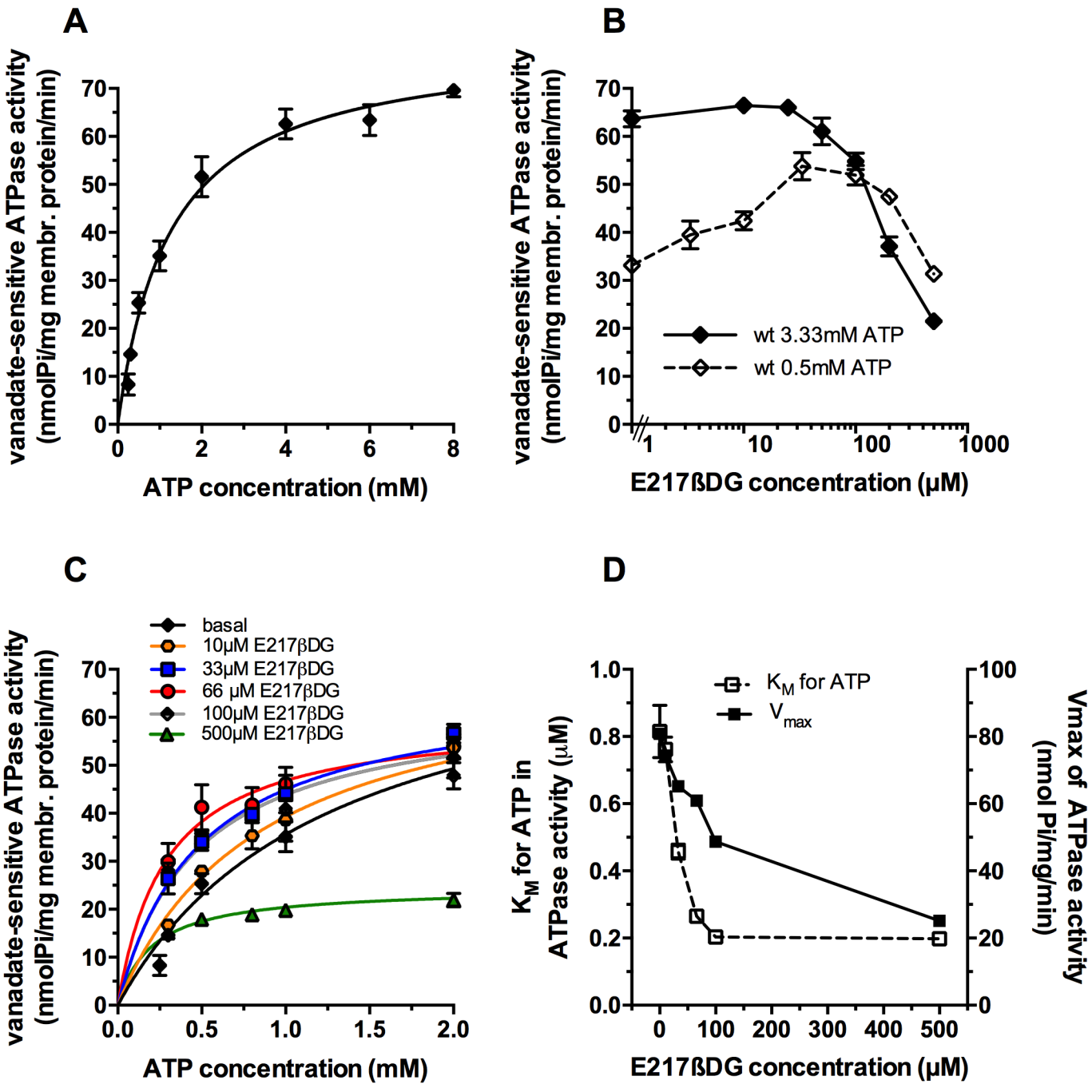
A
vanadate-sensitive ATPase activity (nmolPi/mg membr. protein/min)
ATP concentration (mM)
B
vanadate-sensitive ATPase activity (nmolPi/mg membr. protein/min)
wt 3.33mM ATP
wt 0.5mM ATP
E217ßDG concentration (µM)
C
basal
10µM E217βDG
33µM E217βDG
66 µM E217βDG
100µM E217βDG
500µM E217βDG
vanadate-sensitive ATPase activity (nmolPi/mg membr. protein/min)
ATP concentration (mM)
D
K_M for ATP
V_max
K_M for ATP in ATPase activity (µM)
Vmax of ATPase activity (nmol Pi/mg/min)
E217ßDG concentration (µM)

Figure 3.

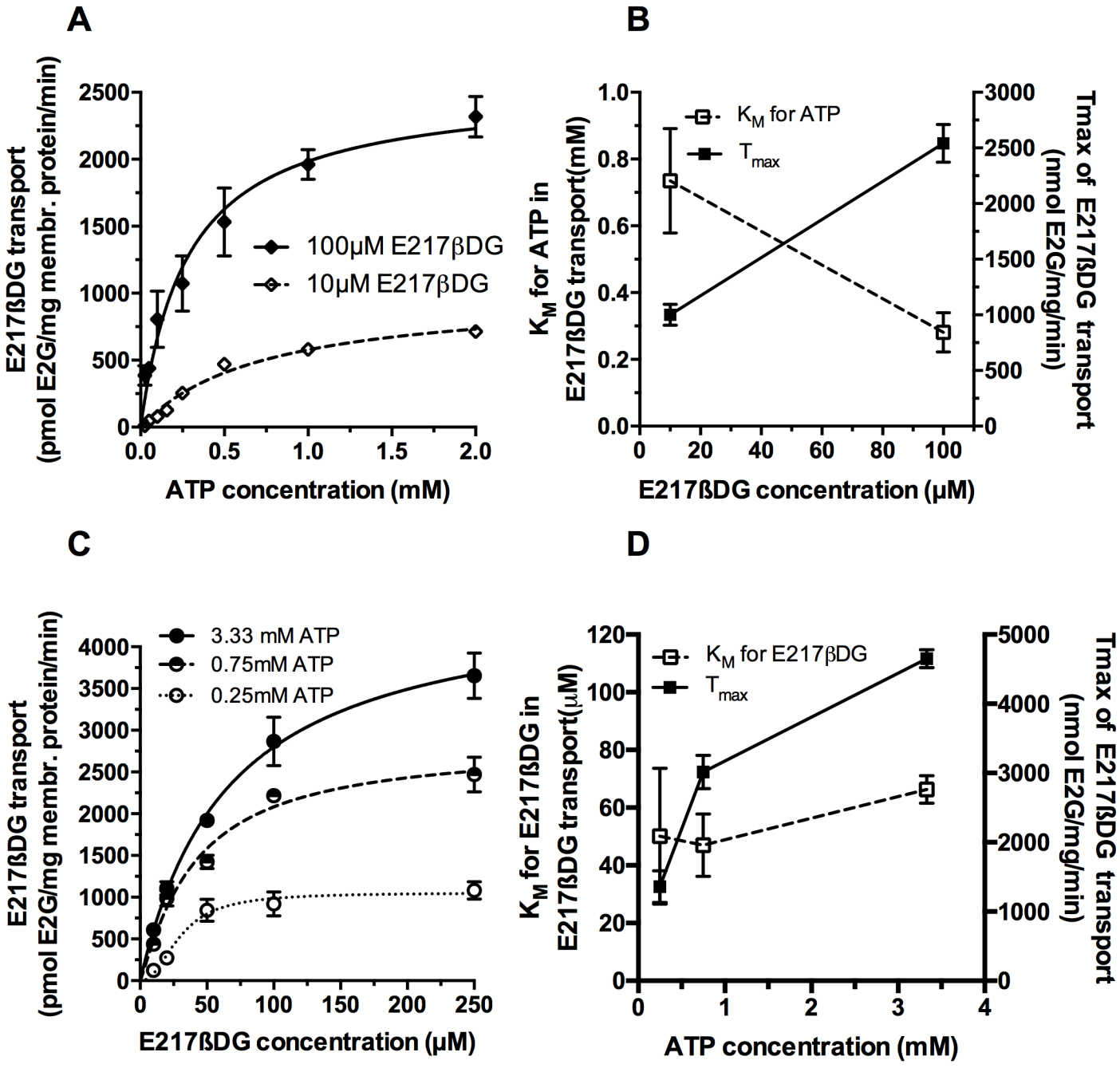
A
E217ßDG transport
(pmol E2G/mg membr. protein/min)
2500
2000
1500
1000
500
0
0.0
0.5
1.0
1.5
2.0
ATP concentration (mM)
100µM E217βDG
10µM E217βDG
B
K_M for ATP
T_max
K_M for ATP in
E217ßDG transport(mM)
1.0
0.8
0.6
0.4
0.2
0.0
0
20
40
60
80
100
E217ßDG concentration (µM)
3000
2500
2000
1500
1000
500
0
Tmax of E217ßDG transport
(nmol E2G/mg/min)
C
3.33 mM ATP
0.75mM ATP
0.25mM ATP
E217ßDG transport
(pmol E2G/mg membr. protein/min)
4000
3500
3000
2500
2000
1500
1000
500
0
0
50
100
150
200
250
E217ßDG concentration (µM)
D
K_M for E217βDG
T_max
K_M for E217ßDG in
E217ßDG transport(µM)
120
100
80
60
40
20
0
0
1
2
3
4
ATP concentration (mM)
5000
4000
3000
2000
1000
0
Tmax of E217ßDG transport
(nmol E2G/mg/min)

Figure 4.

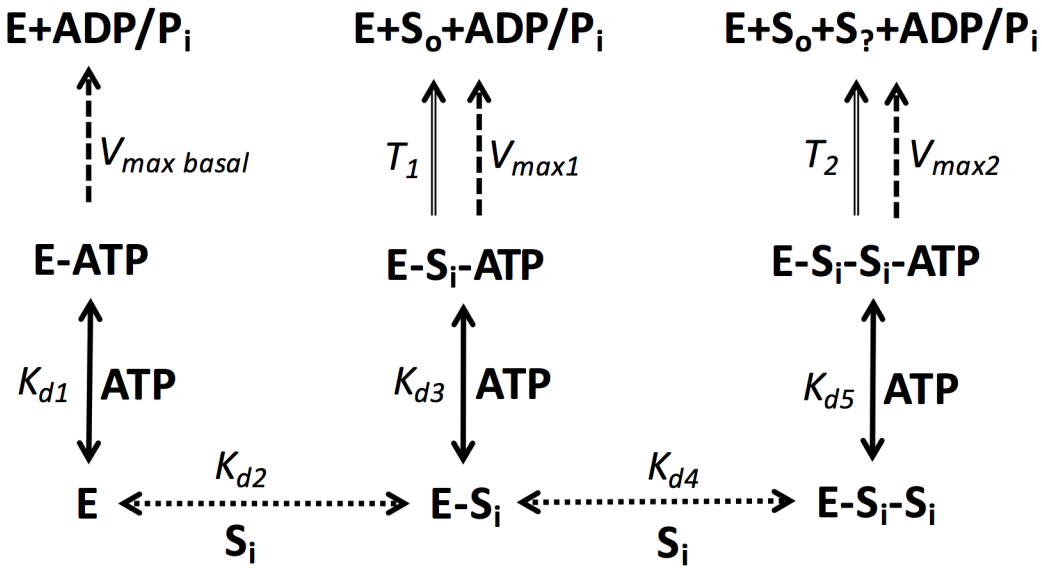
E+ADP/Pi
E+So+ADP/Pi
E+So+S?+ADP/Pi
Vmax basal
T1
Vmax1
T2
Vmax2
E-ATP
E-Si-ATP
E-Si-Si-ATP
Kd1
ATP
Kd3
ATP
Kd5
ATP
Kd2
Kd4
E
E-Si
E-Si-Si
Si
Si

Figure 5.

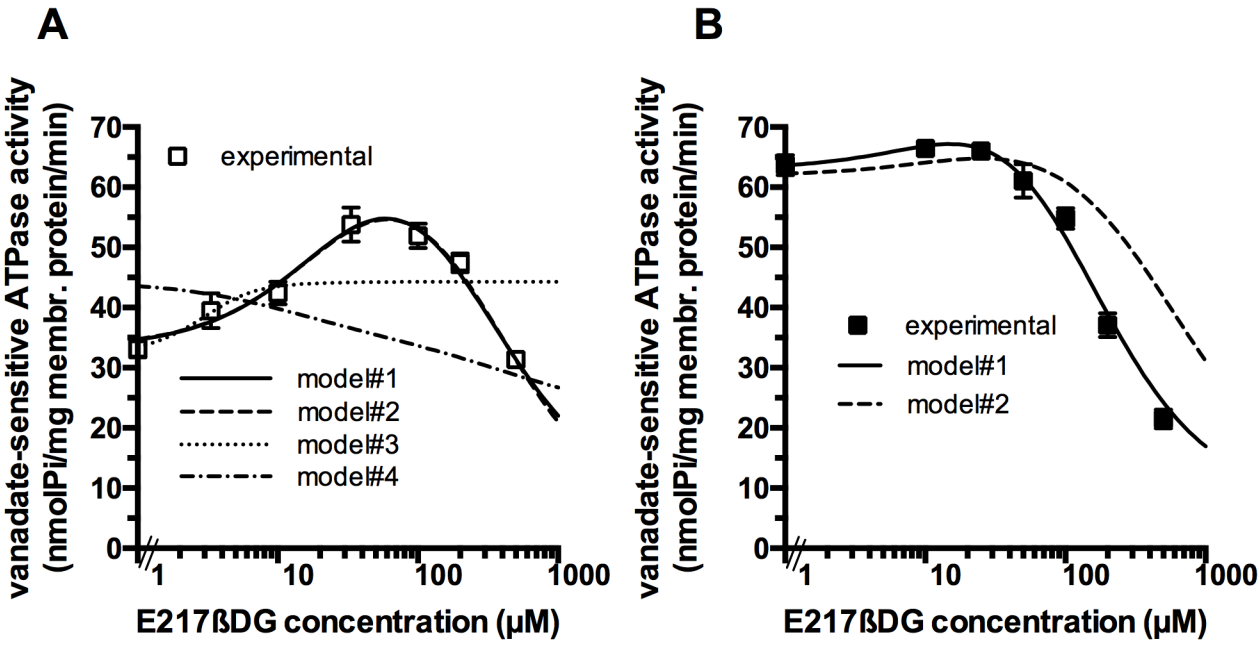
A
B
vanadate-sensitive ATPase activity (nmolPi/mg membr. protein/min)
E217ßDG concentration (µM)
experimental
model#1
model#2
model#3
model#4
0
10
20
30
40
50
60
70
1
10
100
1000

Figure 6.

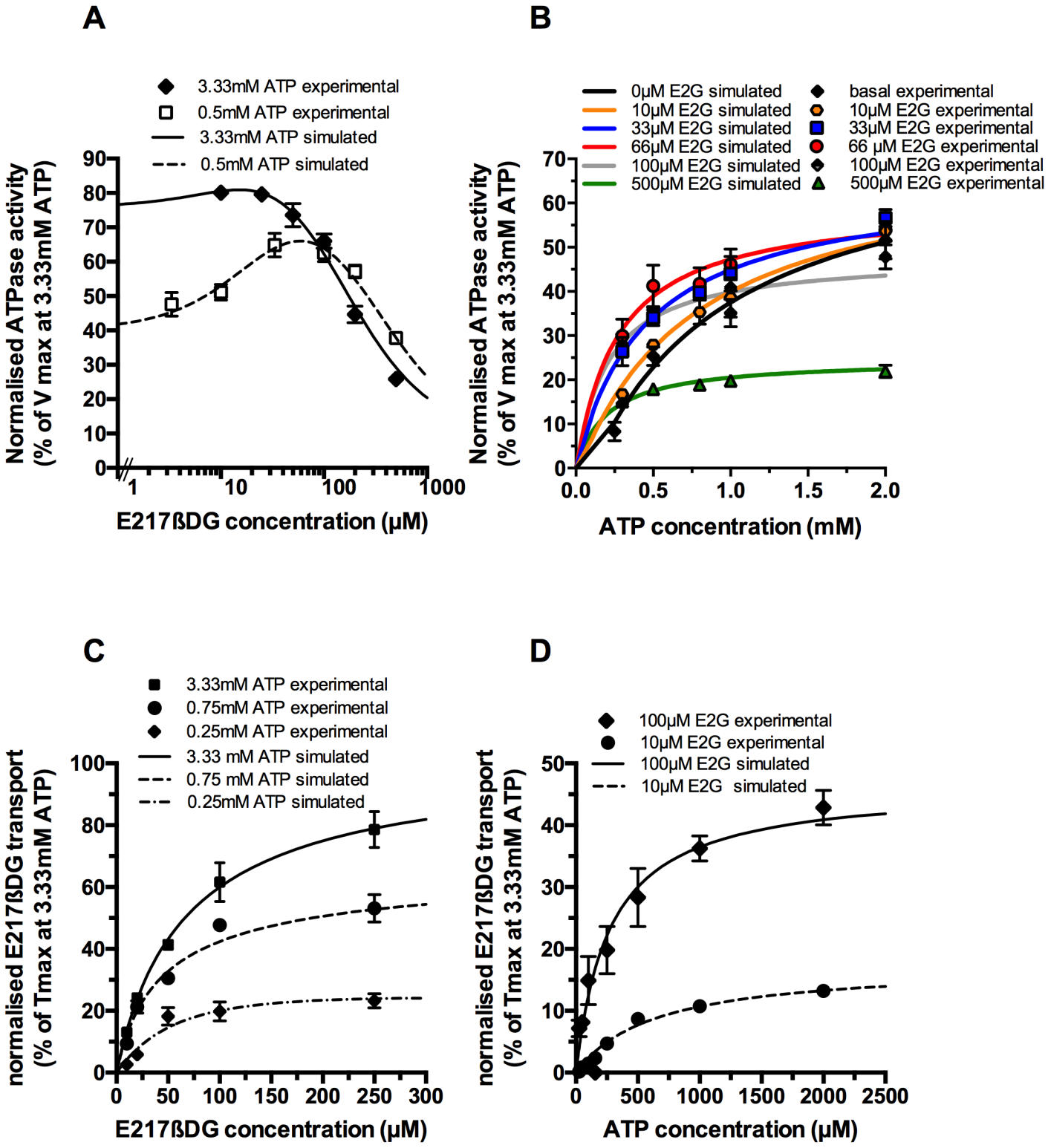
A
3.33mM ATP experimental
0.5mM ATP experimental
3.33mM ATP simulated
0.5mM ATP simulated
Normalised ATPase activity (% of V max at 3.33mM ATP)
E217ßDG concentration (µM)
B
0µM E2G simulated
10µM E2G simulated
33µM E2G simulated
66µM E2G simulated
100µM E2G simulated
500µM E2G simulated
basal experimental
10µM E2G experimental
33µM E2G experimental
66 µM E2G experimental
100µM E2G experimental
500µM E2G experimental
Normalised ATPase activity (% of V max at 3.33mM ATP)
ATP concentration (mM)
C
3.33mM ATP experimental
0.75mM ATP experimental
0.25mM ATP experimental
3.33 mM ATP simulated
0.75 mM ATP simulated
0.25mM ATP simulated
normalised E217ßDG transport (% of Tmax at 3.33mM ATP)
E217ßDG concentration (µM)
D
100µM E2G experimental
10µM E2G experimental
100µM E2G simulated
10µM E2G simulated
normalised E217ßDG transport (% of Tmax at 3.33mM ATP)
ATP concentration (µM)

Table 1.

A

ATPase activity/ cooperativity		0.5mM ATP			
		Model#			
parameter	dimension	#1	#2	#3	#4
K_{d1}	µM	815*	815*	815*	815*
K_{d2}	µM	100	97	319	500
K_{d3}	µM	100	97	815	815
K_{d4}	µM	176	86	10	500
K_{d5}	µM	176	815	10	815
$V_{max\ basal}$	nmol Pi/mg/min	87	88	83	117
V_{max1}	nmol Pi/mg/min	89	87	90	90
V_{max2}	nmol Pi/mg/min	10	10	45	60
R		0.988	0.927	0.548	-0.185
Chi^2		0.13	0.12	3.92	12.23

B

ATPase activity/ cooperativity		3.33mM ATP	
		Model#	
parameter	dimension	#1	#2
K_{d1}	µM	815*	815*
K_{d2}	µM	118	117
K_{d3}	µM	118	117
K_{d4}	µM	131	815
K_{d5}	µM	131	102
$V_{max\ basal}$	nmol Pi/mg/min	78	77
V_{max1}	nmol Pi/mg/min	82	72
V_{max2}	nmol Pi/mg/min	8	10
R		0.996	0.971
Chi^2		0.31	10.35

Model #1 Both ATP are cooperative. (K_{d2}=K_{d3}; K_{d4}=K_{d5})

Model #2 1st ATP is cooperative (K_{d2}=K_{d3})

Model #3 2nd ATP is cooperative (K_{d4}=K_{d5})

Model #4 Neither ATP are cooperative

*Fixed value

Table 2.

A

ATPase activity		E2G dependence		ATP dependence						Model#1	
parameter	dimension	0.5 mM ATP	3.3 mM ATP	0 µM E2G	10 µM E2G	33 µM E2G	66 µM E2G	100 µM E2G	500 µM E2G	Average	SD
K_{d1}	µM	815*	815*	815*	815*	815*	815*	815*	815*	**815***	
K_{d2}	µM	100	118	163	200	200	170	156	200	**163**	**38**
K_{d3}	µM	100	118	163	200	200	170	156	200	**163**	**38**
K_{d4}	µM	176	131	87	107	107	127	107	182	**128**	**34**
K_{d5}	µM	176	131	87	107	107	127	107	182	**128**	**34**
$V_{max\ basal}$	nmol Pi/mg/min	87	78	73	71	71	71	98	71	**78**	**10**
V_{max1}	nmol Pi/mg/min	89	82	88	70	70	78	87	70	**79**	**8**
V_{max2}	nmol Pi/mg/min	10	8	11	8	8	8	8	8	**9**	**1**
R		0.988	0.996	0.993	0.996	0.997	0.996	0.997	0.997	**0.995**	**0.003**
Chi^2		0.13	0.31	4.3	0.61	0.16	0.24	0.26	0.1	**0.764**	**1.438**

B

E2G transport activity		E2G dependence			ATP dependence		Model#1	
parameter	dimension	3.3 mM ATP	0.75 mM ATP	0.25 mM ATP	10 uM E2G	100 uM E2G	mean	SD
K_{d1}	µM	815*	815*	815*	815*	815*	**815***	
K_{d2}	µM	142	108	144	157	152	**141**	**19**
K_{d3}	µM	142	108	144	157	152	**141**	**19**
K_{d4}	µM	142	153	184	205	193	**175**	**27**
K_{d5}	µM	142	153	184	205	193	**175**	**27**
T_1	nmol E2G/mg/min	0.51	0.48	0.53	0.71	0.65	**0.58**	**0.10**
T_2	nmol E2G/mg/min	1.06	0.8	0.37	0.49	0.34	**0.61**	**0.31**
R		0.999	0.988	0.973	0.995	0.99	**0.989**	**0.01**
Chi^2		0.00075	0.0078	0.0102	0.0148	0.0079	**0.00829**	**0.005**

C

Model#1		Integrated values	
parameter	dimension	mean	SD
K_{d1}	µM	**815***	
K_{d2}	µM	**155**	**33**
K_{d3}	µM	**155**	**33**
K_{d4}	µM	**146**	**39**
K_{d5}	µM	**146**	**39**
$V_{max\ basal}$	nmol Pi/mg/min	**78**	**10**
V_{max1}	nmol Pi/mg/min	**79**	**8**
V_{max2}	nmol Pi/mg/min	**9**	**1**
T_1	nmol E2G/mg/min	**0.58**	**0.1**
T_2	nmol E2G/mg/min	**0.61**	**0.31**

*Fixed value